Energy Conversion and Management 313 (2024) 118614

Contents lists available at ScienceDirect

Energy Conversion and Management

journal homepage: www.elsevier.com/locate/enconman

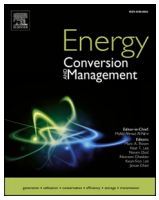

Hydrodynamic characteristics and parametric optimizations of a hybrid system combining a hinged wave energy converter and a breakwater with a semi-opened moonpool

Fukai Song [a], Yong Cheng [a], Saishuai Dai [b,*], Zhiming Yuan [a,b], Atilla Incecik [b]

[a] School of Naval Architecture and Ocean Engineering, Jiangsu University of Science and Technology, Zhenjiang 212003, China
[b] Naval Architecture, Ocean and Marine Engineering Department, University of Strathclyde, Glasgow, United Kingdom

ARTICLE INFO

Keywords:
Wave energy conversion
Floating breakwater
Semi-opened moonpool
Multi-degree-of-freedom
Coupled effect

ABSTRACT

Combining a Wave Energy Converter (WEC) with a floating breakwater to enhance both wave attenuation and the energy capture performance is a plausible pathway to commercializing wave energy technologies. The research introduced a new integrated system that merges a hinged wave energy converter and a breakwater with a semi-opened moonpool. Both the breakwater and the WEC were investigated using multi-Degrees-of-Freedom (DOF) to incorporate a realistic coupling between the two. These two systems were connected through an articulated Power-Take-Off mechanism, and power was harnessed through their relative pitching motion induced by wave loads. The study utilized the Finite Volume Method (FVM) to develop a three-dimensional (3-D) numerical wave tank (NWT) and analyzed the hydrodynamic characteristics of the proposed hybrid system under regular wave loading. Subsequently, design parameters of the two devices, such as the length of the breakwater caisson and the bottom shape of the WEC, were optimized to improve the system's performance. The results indicated that the combination of the two devices enhanced both wave attenuation and energy conversion capacity, compared to using a standalone WEC or breakwater. Notably, the wave power absorption demonstrated a broader effective frequency bandwidth and a higher capture width ratio.

1. Introduction

Along with continuously increasing electricity demand, the problems of environmental pollution are becoming increasingly prominent, Net-Zero becomes a critical strategic development plan worldwide. Total global electricity generation in 2050 is expected to be more than 2.5 times the current level, with nearly 90 % of electricity generation coming from renewable sources [1]. The European Commission [2] believes that wave energy, with its wide distribution, large reserves and predictability [3], is an important direction for future energy development. To capture the wave energy, a series of Wave Energy Converters (WEC) have been invented, including OverTopping (OT) type: OBREC [4], Oscillating Water Column (OWC) type: Uniwave [5] and REWEC3 [6], and Oscillating Buoy (OB) type: WaveRoller [7], Dolphin [8] and LAMWEC [9].

Among various WECs, OB is a typical type that has been extensively studied [10]. Zhang et al. [11] employed Computational Fluid Dynamics (CFD) software to study the hydrodynamic characteristics of oscillating-buoy WECs with different geometries. It is concluded that asymmetric floaters, particularly the streamlined bottom devices, performed better in energy capture and wave attenuation. Ning et al. [12] investigated a vertical pile-supported OB experimentally and validated the advantages of the OB with a long front wall for wave blocking effect. In recent years, multi-body articulated WECs have become increasingly popular, e.g., the multi-mode line absorber M4 [13] and the McCabe device [14,15]. Zheng et al. [16] presented a WEC system that combined two interconnected floaters and a linear Power Take-Off (PTO) system. The maximum wave energy conversion of the system was evaluated based on a 3-D wave radiation-diffraction theory. As an extension of this study, Zheng and Zhang [17] analytically probed the effect of the fore-and-aft float length ratio. The study found that the combination of a shorter fore floater and a longer aft floater benefits energy extraction. Yu et al. [18] established the viscous modified potential flow theory method to investigate the motion response of an Anti-pitch Generating Wave Energy Converter (AGWEC) and used CFD simulation to validate the proposed method. Wang et al. [19] optimized the structure of two hinge-

* Corresponding author.
E-mail address: saishuai.dai@strath.ac.uk (S. Dai).

https://doi.org/10.1016/j.enconman.2024.118614
Received 29 February 2024; Received in revised form 29 April 2024; Accepted 27 May 2024
Available online 8 June 2024

barge WECs by numerical analysis and wave flume experiments. The experimental data identified that a proper design of the damping plate under the rear floater can promote the energy capture of the device.

Nevertheless, high maintenance costs and low conversion efficiency have impeded the commercialization of WECs. Some studies have proposed combining WECs and existing marine structures to reduce the costs of maintenance and installation. Offshore wind energy and wave energy usually coexist because of the natural correlation. As a result, it is possible to integrate offshore wind turbines and WECs [20,21]. A 'TWWC' model combined with a wind turbine with a heaving-type WEC was developed by Ren et al. [22], and scale model experiments were used to prove the reliability of the numerical model. Wan et al. [23] numerically studied three systems of wind turbines and WECs proposed for different water depth conditions, finding that the hybrid system integrating two types of renewable energy generation devices can increase the maximum output power by more than 10 %. The motion response of a wind turbine with WECs was studied based on multi-body constraint dynamics by Zhou et al. [24] confirmed that at the resonant period, the motion of WECs reduces that of the platform. Additionally, Cheng et al. [25] integrated a multi-degree-of-freedom WECs system into a semi-submersible wind turbine platform and demonstrated that it is viable to combine different types of WECs into floating wind turbine platforms numerically and experimentally. Tian et al. [26] studied a WEC type wind turbine system in different configurations (e.g., number of WECs vs number of floating wind turbines). The numerical results showed that the optimal performance is achieved through the combination has three WECs.

On the other hand, due to the excellent compatibility of breakwaters and WECs, their integration is also an attractive option for wave energy development and wave attenuation. He et al. [27] investigated the energy conversion performance of a breakwater with two asymmetric OWCs on the seaside and the leeside, respectively. The results indicated that the breakwater with asymmetric chambers can extend the effective period range without reducing the wave attenuation and the motion response. Zhang et al. [28] proposed a CFD model of a OB-breakwater type dual-floater system and investigated its hydrodynamic performance, demonstrating the better energy capture capability of the combination at long-period waves. Yang et al. [29] adopted a CFD model to investigate the coupling effect between a Wavestar-shaped WEC and a stationary breakwater. They found that the WEC motion increases when standing waves are generated by the fixed breakwater. Cheng et al. [30] proposed a combination of an OB-type breakwater and an OWC and evaluated the influences of wave parameters. More recently, with the development of numerical methods, the hybrid system of breakwaters with irregular shapes and WECs has received attention. Based on N-S equations, Ji et al. [31] numerically investigated a reversed L-type breakwater-WEC system and analyzed the influence factors on the hydrodynamic performance of the breakwater-WEC system. The solution discovered that there exists a suitable PTO damping coefficient that allows the device to achieve optimal conversion efficiency. Cheng et al. [32] proposed a moon-pool type dual-cylinder breakwater and numerically simulated the wave energy capture capacity and the movement characteristics of the system. The results revealed that the integrated system provides better wave attenuation than the individual breakwater. There are also additional programs that combine floating breakwaters or other offshore structures with WECs to realize cost-sharing [33,34].

Despite numerous innovative concepts and extensive research and development activities, the application of WEC has not yet reached a mature commercial stage due to the lack of efficient extraction of energy from the wave field [35]. Integrating multiple WECs to construct wave energy farms is deemed an effective strategy to facilitate the commercialization of wave energy exploitation. Zhang et al. [36] numerically studied the coupled effect of the multi-WECs breakwater system. They found that when the WECs are near the breakwater, the coupled system shows better wave energy conversion performance. Similarly, Tay [37,38] proposed placing WECs in a semi-enclosed moonpool, demonstrating that this integration approach can increase power generation by leveraging the resonance of the moon pool and utilizing the reflection from the moonpool wall.

In this paper, a combination of a WEC with a semi-opened moonpool-type breakwater is proposed to investigate the impact of floating breakwater motions on the hydrodynamic characteristics and wave energy capture performance. Most of the previous studies on the WEC-breakwater hybrid system assumed a fixed breakwater. However, in practical engineering, floating breakwaters have multi-degree-of-freedom movement under wave loads, despite the mooring system. The system configuration is further optimized based on the results of numerical simulation. Additionally, the influence of the geometrical shape of the WEC on the hydrodynamic performance of the system is analyzed in detail. This analysis aims to provide guidance and recommendations for the optimal design of the system in practical engineering applications.

The paper is arranged as follows. In Section 2, the WEC-breakwater numerical model is developed. Section 3 validates the CFD model by comparing it with a series of published papers. The superior performance of the integrated system with side rectangular caissons is illustrated by comparison with a system without side caissons in Section 4. Moreover, the sensitivity of the hydrodynamic performance to caisson width, sub-devices distance, WEC draft and WEC bottom shape was analyzed fully. Finally, the conclusions are summarized in Section 5.

2. Numerical method

2.1. Model and numerical wave tank

The proposed semi-opened moon-pool type breakwater is connected with a WEC through the PTO system, as shown in Fig. 1. The two sub-devices are linked by an articulated mechanism and a hydraulic PTO system as depicted in Fig. 2. Power generation is facilitated by the PTO system through the relative pitching motion induced by the WEC and the breakwater. Both the WEC and the breakwater rotates around the central hinge point o indicated by the red circle in Fig. 2, where L_1 and L_2 are the height from the hinge point o to the draft line of the two floats, respectively. The axial distance between the two floating bodies is expressed as $L = L_3 + L_4$ (when both devices floating in upright condition). The L_5 and the L_6 denote the distance from the ends of the hydraulic piston cylinder to the center hinge point o, L_7 refers to stroke length of the PTO.

The interaction of waves and the proposed hybrid system is simulated using a 3-D NWT for an incompressible viscous fluid, as illustrated in Fig. 2. The NWT length is set at eight times the incident wavelength (λ). A wave-generating zone and a wave-absorbing zone are deployed at each end of the NWT, both have a length of 1.5λ. The NWT is divided

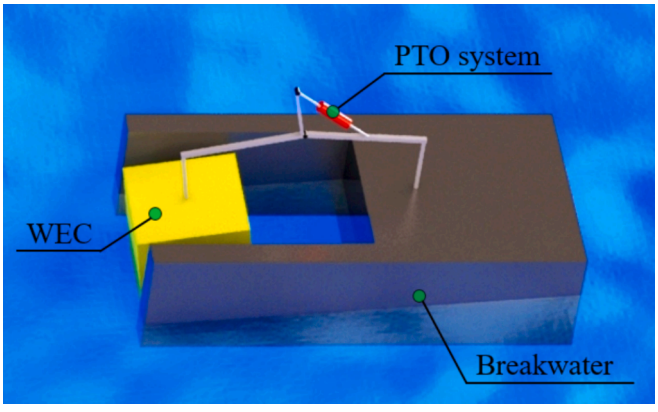

Fig. 1. Bird's view of the WEC-breakwater hybrid system.

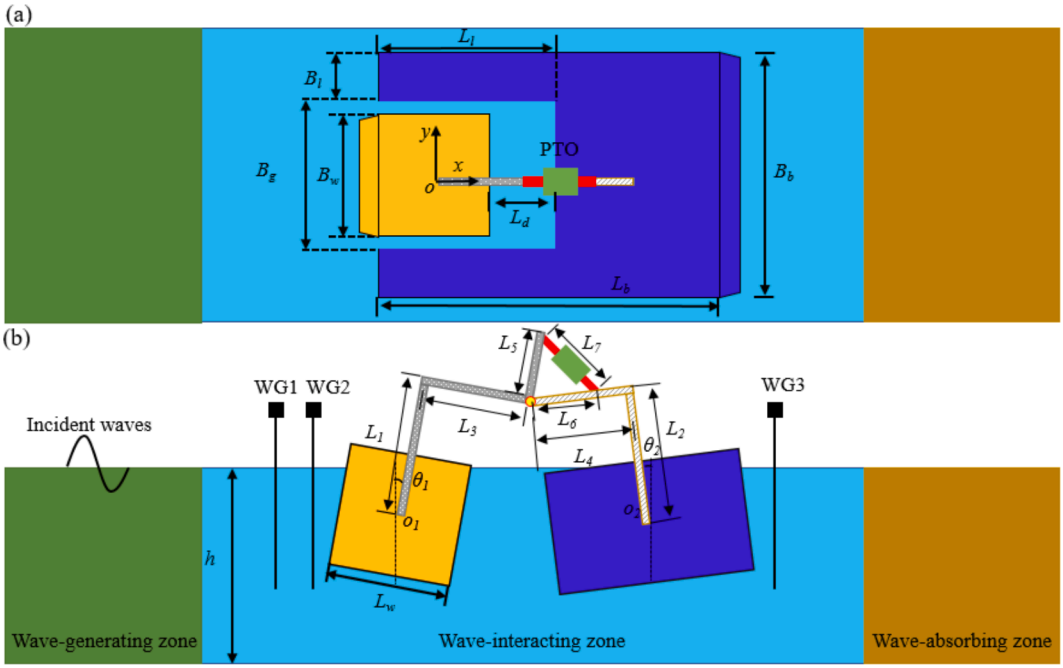

Fig. 2. Schematic of the hybrid system in the NWT: (a) Planform and (b) Profile view.

vertically into the water and gas phases, each defined as twice the water depth (h). The boundary conditions are established, with the left and right sides of the NWT set to velocity inlet, and the top boundary specified as a pressure outlet. Specifically, the velocity inlets are characterized by the velocity of a fifth-order Volume of Fluid (VoF) wave and the hydrostatic pressure of the fifth-order VoF wave [39], respectively. Additionally, a non-slip wall boundary condition is assigned to the bottom of the NWT. To absorb the reflected and radiated waves from the hybrid system, the Euler Overlay Method (EOM) [40] is employed at the velocity inlet boundaries, wherein the method calculates the difference between the theoretical and the actual simulated wave information in the wave generation zone and then enforces the simulated wave to match the theoretical value through the addition of corresponding source or sink terms into the control equations. This source or sink term takes a specific form.

$$q_\phi = -\gamma\rho(\phi - \phi^*) \tag{1}$$

where γ is the forcing coefficient; ρ is the fluid density; the ϕ is the actual solution of the transport equation and the ϕ^* is the analytical solution.

In the wave-absorbing zone, wave damping is achieved by introducing a resistance term to the vertical velocity equation [41]

$$S_z^d = \rho(f_1 + f_2|w|)\frac{e^K - 1}{e^1 - 1}w \tag{2}$$

and

$$K = \left(\frac{x - x_{sd}}{x_{ed} - x_{sd}}\right)^{n_d} \tag{3}$$

where the $Sd\ z$ is the resistance term; f_1, f_2 and n_d are the parameters of the damping model, w is the vertical component of the velocity; K is the amplitude of the wave vector; x_{ed} and x_{sd} are the start point (the left end of the wave-absorbing zone) and the end point (velocity inlet boundary) of the wave damping zone, respectively. The lateral boundaries are given as the symmetrical boundary condition.

2.2. Energy conversion of the integrated system

The breakwater experiences pitch and heave motion under wave loads. Meanwhile, the WEC rotates around the hinged point, and the relative pitch angle of sub-devices is utilized to generate power. The "multi-body motion" is created in the CFD software to simulate the motion of the sub-devices in the system. A rotated joint coupling is established for sub-devices and the equivalent PTO damping moment [0, M_{PTO}, 0] is added at the mass center of the sub-devices respectively. The PTO damping moment M_{PTO} of the linear PTO system which acted on the WEC is described as

$$M_{PTO} = -b_{PTO}(\theta_w' - \theta_b') \tag{4}$$

where θ_w and θ_b are the rotated angles of the two sub-devices, a subscript w denotes the WEC while a subscript of b denotes the breakwater and b_{pto} is the PTO damping coefficient:

$$b_{PTO} = \frac{\sqrt{2}}{2}cL_3^2 \tag{5}$$

where c is the damping coefficient of the hydraulic piston cylinder. Note the difference between the PTO damping and the hydraulic piston damping coefficient is not the same, where the PTO damping has a dimension of Nms/rad while the piston damping has a unit of Ns/m. The motion equations of the hybrid system can be written as the following matrix

$$\begin{bmatrix} m_b & 0 & 0 \\ 0 & I_b & 0 \\ 0 & 0 & I_w \end{bmatrix}\begin{Bmatrix} \zeta'' \\ \theta_b'' \\ \theta_w'' \end{Bmatrix} + \begin{bmatrix} 0 & 0 & 0 \\ 0 & b_{PTO} & 0 \\ 0 & 0 & b_{PTO} \end{bmatrix}\begin{Bmatrix} \zeta' \\ \theta_b' \\ \theta_w' \end{Bmatrix} + \begin{bmatrix} b_{z(b1)} & 0 & 0 \\ 0 & b_{z(b2)} & 0 \\ 0 & 0 & b_{z(w)} \end{bmatrix}\begin{Bmatrix} \zeta' \\ \theta_b' \\ \theta_w' \end{Bmatrix} = \begin{Bmatrix} F_{h(b)} \\ M_{r(b)} \\ M_{r(w)} \end{Bmatrix} \tag{6}$$

where m_b and ς denote the mass and heaving displacement of the breakwater, $F_{h(b)}$ signifies the vertical hydrodynamic force acting on the breakwater; I_b and I_w are the rotational inertia of the WEC and the breakwater, respectively; $b_{z(b1)}$ and $b_{z(b2)}$ are heaving and pitching radiational damping for the breakwater, $b_{z(w)}$ is the radiational damping for the WEC; $M_{r(b)}$ and $M_{r(w)}$ are the moments on breakwater and WEC

due to fluid loads.

The energy conversion performance of the combination is assessed using the conversion efficiency η

$$\eta = \frac{E_p}{E_w} \tag{7}$$

where the E_w and E_p are the incident wave energy within one incident wave period and the average generated power of the hybrid system. E_w and E_p can be calculated by equation (8) and (9), respectively

$$E_w = \frac{1}{16}\frac{\rho g H_i^2 \omega B}{k}\left(1 + \frac{2kh}{\sinh 2kh}\right) \tag{8}$$

B represents the width of the device across the incident waves, H_i is the incident wave height, and h is the water depth.

$$E_p = \frac{b_{PTO}}{nT}\int_t^{t+nT} \xi^2 dt \tag{9}$$

n is the WEC motion cycle number; ξ is the amplitude of the relative pitch angle between sub-devices; T is the incident wave period.

As can be observed in Fig. 2, two wave gauges (WG1 and WG2) are set in front of the hybrid system. The thing to bear in mind is that the spacing between the two wave gauges cannot be half a wavelength or a multiple thereof. Because at those points the wave surface elevation at the two measurement points will be the same while the phase difference will be 180, which makes it impossible to separate the incident and reflected waves. Therefore the spacing between WG1 and WG2 is set as 0.1λ. The WG2 and WG3 are 1λ from the front and end of the hybrid system, respectively. The reflection coefficient K_r and the transmission coefficient K_t of the WEC-breakwater system can be expressed as

$$K_r = \frac{H_r}{H_i} \tag{10}$$

$$K_t = \frac{H_t}{H_i} \tag{11}$$

where H_r and H_t are the reflection wave height and transmission wave height respectively.

2.3. Mesh setup

The overset mesh method offers a precise and convenient approach for handling complex free surface flows. It involves dividing the free surface into distinct sub-domains, which can overlap, allowing for independent calculation of flow within each sub-domain[42]. The overset mesh method is chosen for this study to define the mesh covering the hybrid system. A non-slip wall boundary condition is applied to the object surface, and the surface outside the body is defined as an overset mesh condition. To enhance the solution accuracy, a trimmed mesher model is utilized to divide the area surrounding the free surface into a liquid transition zone and a liquid encryption zone. The prism layer mesher and surface mesher are used to create five primary layers, while the mesh within the motion zone of the system is encrypted, as depicted in Fig. 3.

3. Model validation

3.1. Convergence study

Verification is necessary for numerical simulations. The main parameters of the considered WEC-breakwater hybrid system are as follows: the water depth $h = 0.7$ m, the total breakwater width $B_b/h = 1.11$, the total WEC width $B_w/h = 0.57$, the total breakwater length $L_b/h = 2.21$, the total WEC length $L_w/h = 0.57$, the space distance $L_d/h = 0.57$, the side caisson width $L_l/h = 1.14$, the side caisson width $B_l/h = 0.14$ and the submerged depth $d/h = 0.29$. The damping coefficient of the hydraulic piston cylinder is set as $c = 400$ Ns/m. Model parameters with the incident wave height $H_i/h = 0.11$ and the wave period $T = 1.8$ s. Fig. 4 shows the rotated motion of the WEC and the breakwater with different mesh schemes i.e. Mesh a ($\Delta z = H_i/20$, $\Delta x = H_i/10$), Mesh b ($\Delta z = H_i/30$, $\Delta x = H_i/15$) and Mesh c ($\Delta z = H_i/40$, $\Delta x = H_i/20$). All three mesh schemes achieve temporal convergence at the time step specified as $dt = T/1000$. The rotated motion curves between the sub-devices obtained from mesh b and mesh c show a strong level of agreement, with the differences in phase and amplitude being less than 5 %. Therefore, based on the comparison, it can be inferred that the mesh b and the time step $dt = T/1000$ have achieved satisfactory convergence and are deemed suitable for use in the subsequent numerical simulation.

3.2. Validation of simulating an anti-pitching generating WEC

Jin et al. [43] conducted the experiment on a 1:25 scale designed hinged raft WEC (D-HRWEC) in regular waves to investigate the hydrodynamic performance of the devices, with a wave height $H = 0.05$ m and a wave period $T = 1.55$ s. The schematic of the D-HRWEC is given in Fig. 5(b). Comparisons of relative hinge angle and wave elevation between the present CFD solutions and the experimental results are shown in Fig. 5(a), the uniformity between the present simulation and the experimental results suggests the proposed simulation method is capable of simulating the multipbody WEC accurately.

4. Numerical results and discussions

In this section, the hydrodynamic performance of three different types of breakwater integrated systems is investigated, including a floating breakwater with a semi-opened moonpool, a solid square floating breakwater and a fixed square breakwater. For the floating breakwater with a moonpool case, the caisson width, a WEC layout position and WEC draft are also investigated in detail. Ultimately, the study examines how the bottom shape of the WEC affects the hydrodynamic performance of the integrated system. All findings are obtained

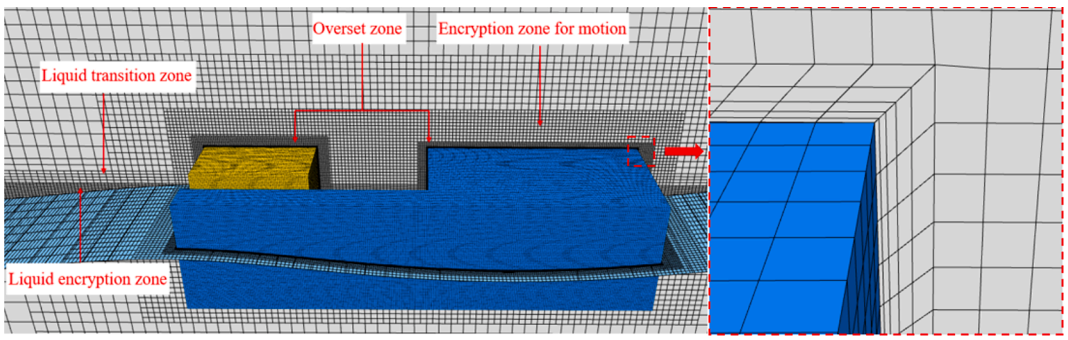

Fig. 3. Typical mesh for the perimeter of the hybrid system.

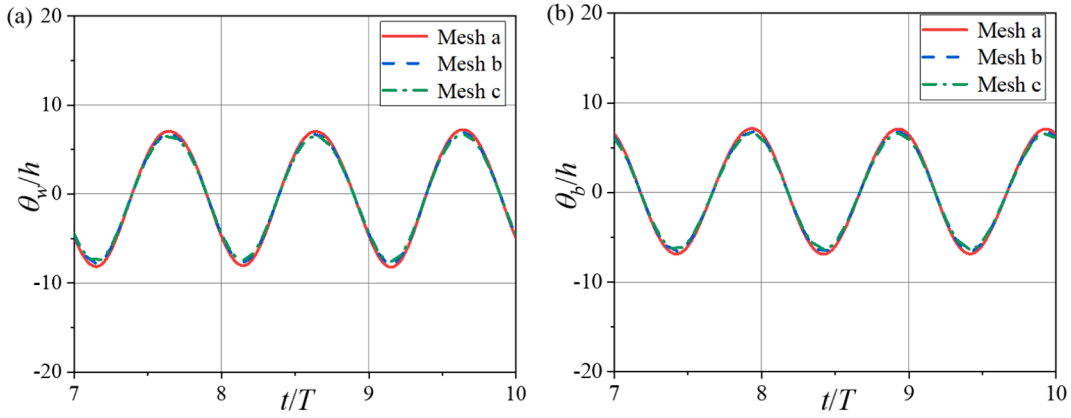

Fig. 4. Convergence study rotated motion of the (a) WEC and (b) floating breakwater.

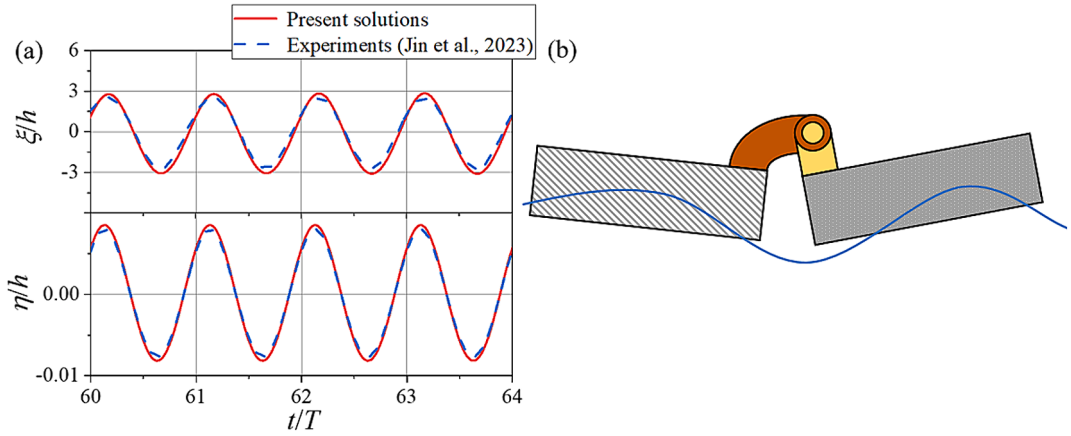

Fig. 5. (a)Time series of the relative hinge angle of the D-HRWEC and the wave elevation; (b) schematic of the D-HRWEC.

from the validated numerical model.

4.1. Comparisons of three different hybrid systems

This study departs from previous research, which primarily concentrated on a WEC integrated onto a fixed-type breakwater. However, it is crucial to consider the installation of a WEC onto a floating breakwater, as it may significantly impact power extraction due to the coupling between the two systems. To investigate this, three different hybrid systems, namely, a WEC with a fixed square breakwater, a WEC with a floating square breakwater (See Fig. 6(a)), and a WEC installed inside the moonpool (See Fig. 6(b)) of a floating breakwater are investigated firstly.

As can be seen in Fig. 7(a)-(b), the relative pitch angle and conversion efficiency of the fixed breakwater system is much higher than that of the floating breakwater system for all wave periods except when the non-dimensional wave period $T(g/h)^{0.5} = 3.7$. It is because at $T(g/h)^{0.5} = 3.7$, the WEC rotation angle is small, and the relative pitch angle is primarily influenced by the floating breakwater rotation angle. In contrast, the movement of the breakwater in the fixed breakwater system is restricted, so the relative pitch angle and conversion efficiency are lower at $T(g/h)^{0.5} = 3.7$. In the region where $T(g/h)^{0.5} > 3.7$, the fixed breakwater system has a stronger wave reflection, resulting in greater WEC motion and higher conversion efficiency. The reflection coefficients in Fig. 7(c) show that in the short-wave period ($6.0 > T(g/h)^{0.5}$), the fixed breakwater system exhibits smaller reflection coefficients compared to the two floating breakwater systems. the opposite trend can be observed in long-wave period ($T(g/h)^{0.5} > 6.7$). This

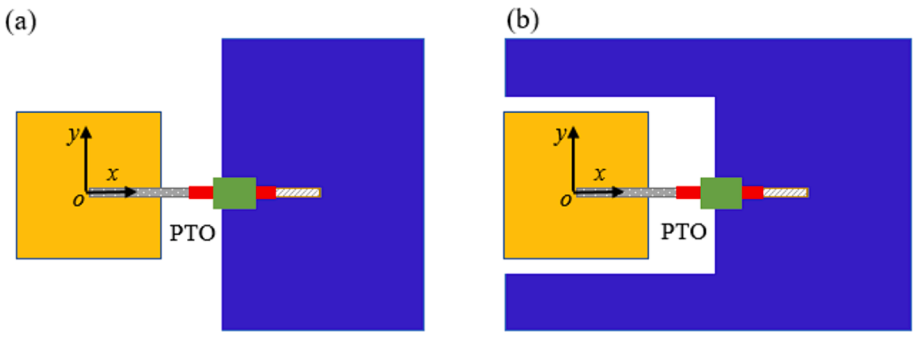

Fig. 6. Schematics of (a) WEC with square breakwater and (b) WEC with semi-opened breakwater.

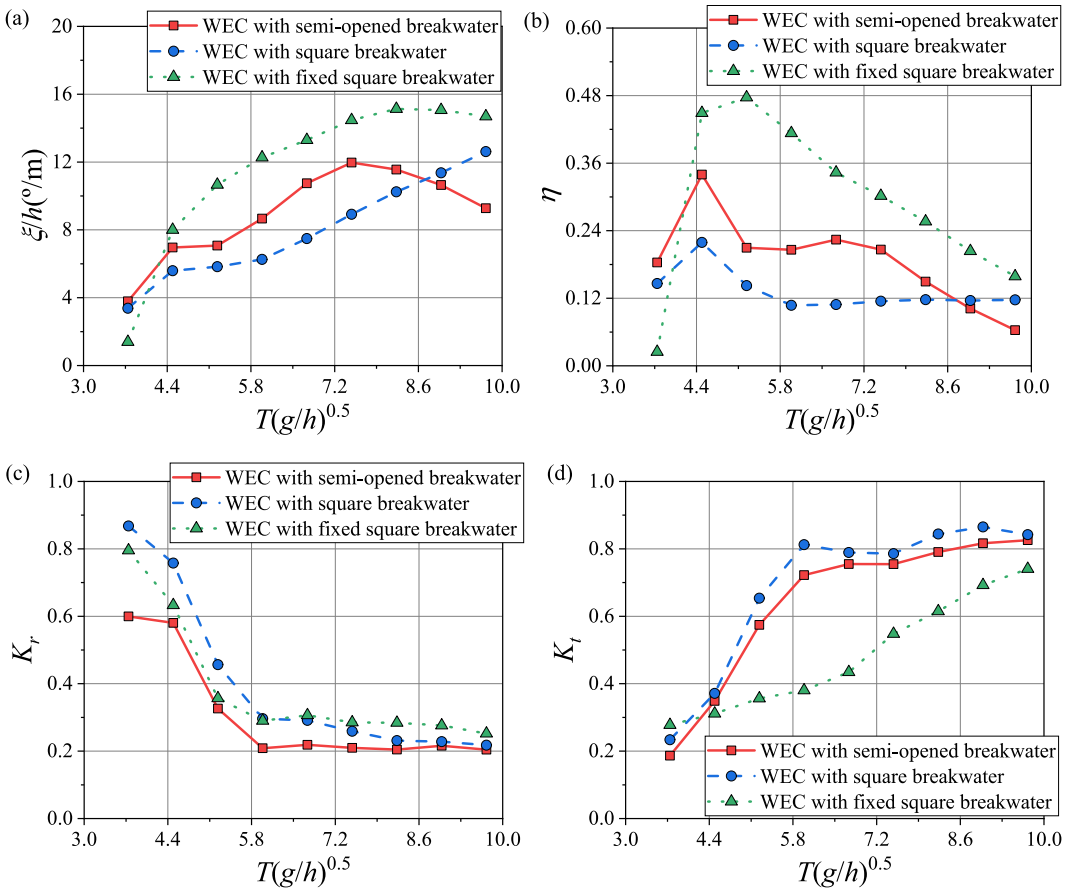

Fig. 7. Comparisons of (a) the relative pitch angle, (b) conversion efficiency, (c) reflection coefficient and (d) transmission coefficient between the three types of hybrid systems.

reversal can be attributed to the enhanced reflection of incident waves by the fixed breakwater. However, the energy harvesting and dissipation of the reflected wave are more significant in the region of short periods. As shown in Fig. 7(d), the fixed breakwater system has better wave attenuation for almost all the wave periods, which corresponds to the energy conversion in Fig. 7(a). The comparison between the fixed breakwater system and the floating breakwater system suggests a fixed breakwater system provides better performance in terms of both energy extraction and wave attenuation.

As a WEC-breakwater system with the function of both energy extraction and wave attenuation, both energy conversion efficiency and wave transmission characteristics are important indicators for evaluating the performance of the integrated system. The hydrodynamic performance of breakwaters with side rectangular caissons was investigated by Wang et al. [44] and Zhao et al. [45,46] respectively, and the results show that the semi-open chamber formed by the side rectangular caisson and back-supporting structure can significantly amplify the wave height inside the chamber. Therefore, this sub-section investigates the effect of the side rectangular caisson structure on wave attenuation and wave energy extraction performance of the hybrid system. The main parameters of cases are kept consistent with that in Section 3.1. As can be observed in Fig. 7(a) and (b), the amplitude of the relative pitch angle of the integrated system with side rectangular caissons is higher in all the wave periods region except for when $T(g/h)^{0.5} > 8.6$, leading to higher wave energy conversion efficiency, proving that the design with side caisson is superior in most working conditions. This may be due to the wave clustering effect of the semi-open chamber formed by the side rectangular caisson structure, and the relative motion of the two sub-devices is increased. In contrast, in the long-period region of $T(g/h)^{0.5} > 8.6$, the relative motion of the system in the long-period wave region is reduced due to the increased length of the breakwater as a result of the designed side caisson structure. Furthermore, the conversion efficiency curve of the hybrid system with side caissons in Fig. 7(b) shows two peaks at $T(g/h)^{0.5} = 4.5$ and $T(g/h)^{0.5} = 6.7$, respectively. This is associated with the dissimilar resonant periods that the two sub-devices have. The conversion efficiency is related to the relative pitch angle, which in turn is affected by the rotated motion of the two sub-devices. When the resonant periods of the sub-devices are different, the conversion efficiency may increase around the respective resonant periods, i.e. the efficiency curve peaks. The efficiency curve of the system without side caissons has only one peak, which indicates that the natural frequencies of the WEC and the square breakwater are similar.

To compare the effect of different designs on the wave attenuation capacity of hybrid systems, Fig. 7 (c) and (d) compare the reflection and transmission coefficient curves of two hybrid systems. The reflection coefficient and transmission coefficient of the combination with side caissons are lower than those of the other across the entire simulated wave period region. This is because more energy is extracted by the case with side caissons, leaving less wave to be reflected and transmitted. There is only a peak in the curve of the system without side caissons, this indicates that the natural frequencies of the WEC and the square breakwater are similar.

In addition to this, the geometric dimensions and configuration, space distance, draft, etc. can also affect the performance of the combination. The chamber structure formed by the side caisson design makes the system superior in efficiency and wave attenuation, as evidenced by the above comparisons in this sub-section. Further numerical simulation and discussion of these parameters will be addressed in subsequent studies.

4.2. Efficiency gain effect from long caisson width

The motion response of the integrated system is significantly influenced by the side caisson structure, as previously discussed in Section 4.1. In order to evaluate the impact of the side caisson, three distinct models with varying caisson widths (B_l/h = 0.14, 0.11 and 0.07) are included in the analysis. It is important to note that from the beginning of this section, the models are systems of WEC with semi-opened breakwaters.

The variation of the relative pitch response amplitude operator (RAO) ξ/h, conversion efficiency η, rotated RAO of WEC ξ_w/h, rotated RAO of breakwater ξ_b/h, reflection coefficient K_r and transmission coefficient K_t for the three models with different caisson widths are shown in Fig. 8. It should be noticed that the relative pitch angle is not obtained by adding rotated angle amplitudes of WEC and breakwater simply, but we can still derive some patterns below from the comparison of the rotated angle amplitudes of the sub-devices in different hybrid systems. Fig. 8(a) and (b) show that the peak conversion efficiencies of three different models are similar, close to 35 %. The different caisson widths did not change the period at which the peak conversion efficiency occurred. An intriguing observation emerges when comparing the efficiency curves of different caisson widths across medium-period ($5.2 < T(g/h)^{0.5} < 7.5$) and long-period waves ($7.5 < T(g/h)^{0.5}$). The trends exhibit an inverse relationship between the two wave regimes. This phenomenon can be elucidated by the limited transmission of medium-period waves to the structure, resulting in the accumulation of energy within the chamber due to impedance from the breakwater. Specifically, in medium-period waves, a reduction in chamber length intensifies

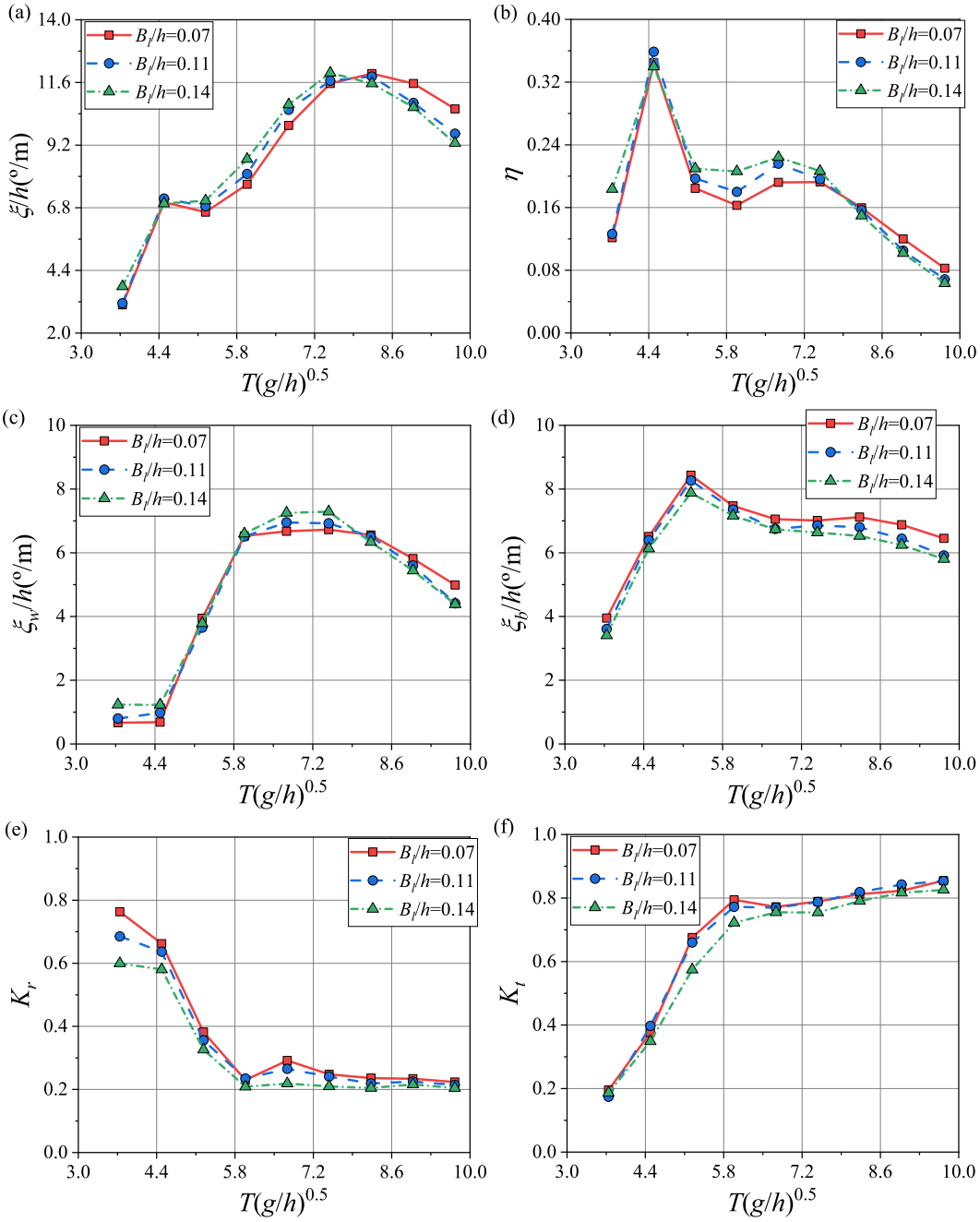

Fig. 8. Comparisons of (a) relative pitch angle, (b) conversion efficiency, (c) rotated angle of WEC, (d) rotated angle of breakwater, (e) reflection coefficient and (f) transmission coefficient for different caisson width.

water resonance effects, while a longer chamber mitigates such effects, thus influencing the efficiency.

As can be seen that the trend of WEC's rotation angle curves with different caisson widths in Fig. 8(c) is the same as that in Fig. 8(b), that is, the effect of caisson width variation on the conversion efficiency of the system in different wave periods is reflected by the variation of WEC motion amplitude. From Fig. 8(d), it is confirmed that the rotated angle of the breakwater decreases as the caisson becomes longer. This is closely related to the fact that the increase in caisson width leads to an increase in the mass of the breakwater, which reduces the motion response of the breakwater.

Fig. 8(e) and (f) illustrate the reflection and transmission coefficients against wave period for different caisson widths. It needs to be explained that when a caisson is introduced, due to the reflection of the radiated wave from the WEC inside the moonpool, the reflected wave might not have uniform wave height across the width of the breakwater. It is verified that the distance of 1λ between WG2 and the front of the caisson is sufficient to eliminate the effects of radiated wave reflections of the WEC in the moon pool. It is clear from Fig. 8(e) that the reflection coefficient of the hybrid system monotonically decreases as the caisson width becomes longer. The key reason may be the fact that total wave reflection is divided into two parts consisting of reflections caused by the side caisson and WEC respectively. Nevertheless, there is a phase difference that leads to the dissipation of the reflected wave between the two parts of the reflected wave height because of the different motions of the sub-devices. An increase in caisson width results in an increase in the effective wave-facing area of the caisson and results in greater wave dissipation. On the other hand, the reflection coefficient curves present similar characteristics as the variation of breakwater rotation angle with caisson width in Fig. 8(d). The reason for this phenomenon is that the

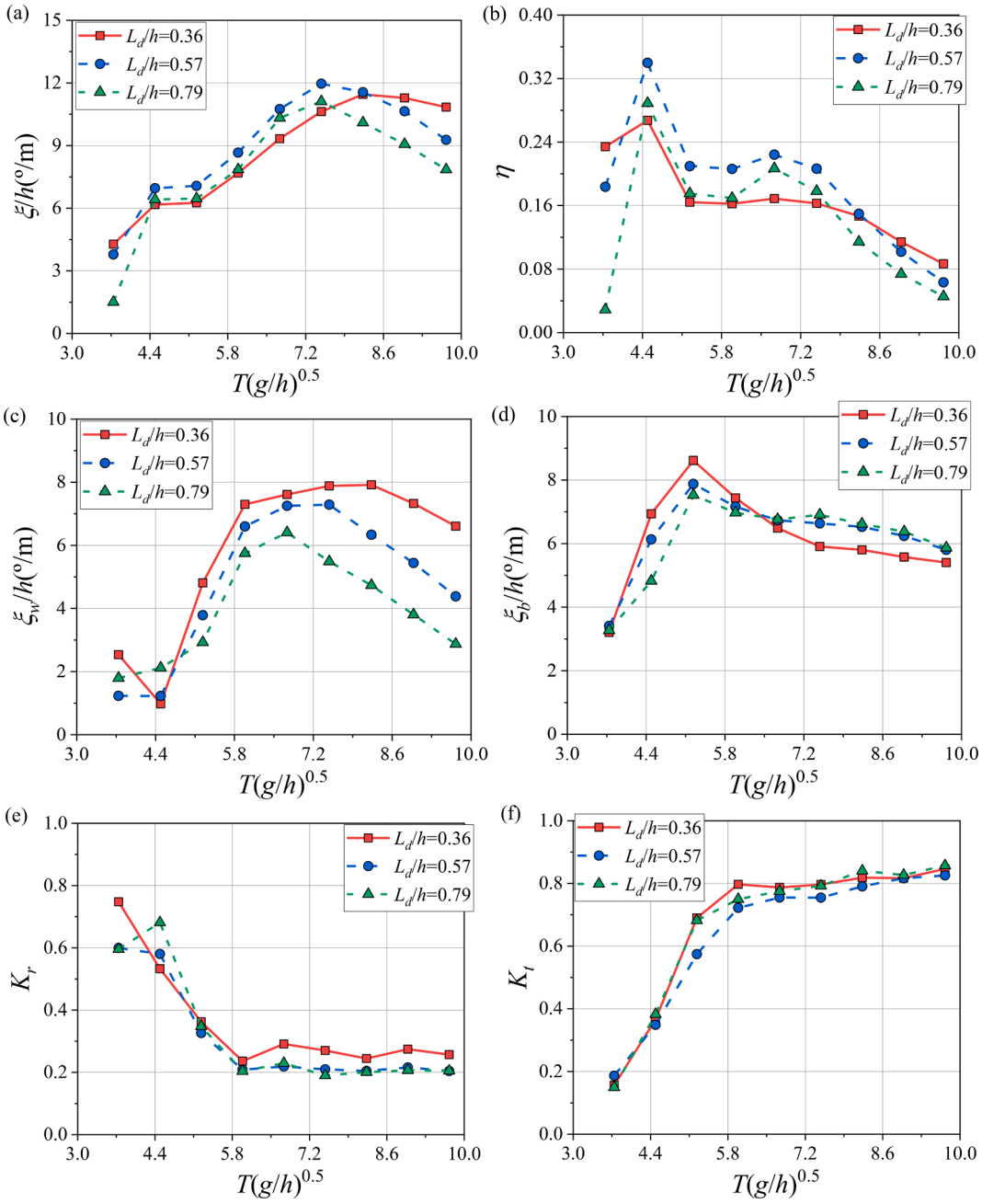

Fig. 9. Variation of (a) relative pitch angle, (b) conversion efficiency, (c) rotated angle of WEC, (d) rotated angle of breakwater, (e) reflection coefficient and (f) transmission coefficient with wave periods at varying spacing distances between sub-devices.

reduction of the caisson reduces the mass of the breakwater, and the breakwater has a greater motion amplitude which leads to larger radiated waves. As plotted in Fig. 8(f), wider caissons result in better wave absorption performance in short-period waves region ($T(g/h)^{0.5} < 6.7$), which can be attributed to that increasing the caisson width results in a larger effective facing-wave area of the system. Whereas long-period waves are easily transmitted over the breakwater, different caisson widths have little effect on the wave dissipation performance, so the transmission coefficient curves almost overlap each other. In summary, the hybrid system with wider caissons has better wave attenuation and a broader effective period range while maintaining peak efficiency. The excellent and comprehensive performance makes it an excellent choice for practical projects.

4.3. Effect of the layout location of the WEC relative to the breakwater

The sub-section examines the effects of the spacing distance between two sub-devices i.e. $L_d/h = 0.36$, 0.57 and 0.79. All other dimensions remain unchanged. Fig. 9 shows the relative pitch RAO ξ/h, conversion efficiency η, rotated RAO of WEC ξ_w/h, rotated RAO of breakwater ξ_b/h, reflection coefficient K_r and transmission coefficient K_t as a function of dimensionless wave period $T(g/h)^{0.5}$ and gap distances between the WEC and the breakwater.

It is emphasized in Fig. 9(a) that for $T(g/h)^{0.5} < 4.5$ and $8.2 < T(g/h)^{0.5}$, the relative pitch angles decrease with the increasing spacing distance, and follow a different trend for the wave period region of $4.5 < T(g/h)^{0.5} < 8.2$. This can be explained by the water column in the chamber resonating near the medium-period region, increasing the relative pitch angle. It is worth mentioning that the hybrid system has the largest relative pitch angles in the medium-period wave range ($4.5 < T(g/h)^{0.5} < 7.5$) when the spacing distance is the same as the length of WEC, corresponding to the largest conversion efficiency in this wave period region as plotted in Fig. 9(b), with a maximum $\eta = 34$ %. In addition, the conversion efficiency curves become steeper as the distance increases.

In Fig. 9(c) the rotated angle of WEC decreases with increasing distance, this can be interpreted as the increase in required torque for WEC rotation due to increasing spacing distance. In contrast, the rotated motion of the breakwater has different sensitivities to spacing distance changes in the long-period region and short-period region as shown in Fig. 9(d). The rotated angle of the breakwater declines with the spacing distance increases in $T(g/h)^{0.5} < 5.3$ and shows an opposite characteristic in $T(g/h)^{0.5} > 5.3$.

Fig. 9(e) shows that the reflection coefficient is greatest at $L_d/h = 0.36$, which is caused by more radiated waves generated from the violent motion of the WEC. The transmission coefficients are less affected by spacing distance in the region of $T(g/h)^{0.5} < 4.5$ and $8.2 < T(g/h)^{0.5}$ as shown in Fig. 9(f), which can be interpreted as the influence of the increase in conversion efficiency in this period range. Comparing Fig. 9(b) and Fig. 9(f), the hybrid system with a dimensionless spacing distance of $L_d/h = 0.57$ is the best choice in terms of expanding the effective frequency bandwidth and improving the wave attenuation performance of the system. In addition, the peak periods of the WEC rotated angle curves decrease with the increasing distance, but the two peak periods of the conversion efficiency are not changed. This demonstrates that the conversion efficiency of the hybrid system is a result of the combined effect of the two sub-devices and the hydrodynamic performance characteristics of an individual sub-device are not necessarily reflected in that of the hybrid system.

4.4. Stable energy conversion from deeper WEC draft

As is well-known, the WEC draft has a significant effect on the resonant period and wave energy extraction of the hybrid system. In this sub-section, three different WEC drafts of $d/h = 0.21$, 0.29 and 0.36 are considered to investigate the influence of dimensionless WEC draft d/h on the wave attenuation and energy extraction performance of the hybrid system. The mass of the WEC changes with displacement. Fig. 10 shows the variation of the relative pitch RAO ξ/h, conversion efficiency η, rotated RAO of WEC ξ_w/h, rotated RAO of breakwater ξ_b/h, reflection coefficient K_r and transmission coefficient K_t with dimensionless wave period $T(g/h)^{0.5}$ for different WEC drafts.

As can be observed from Fig. 10(a) and (b), the WEC draft has an insignificant effect on relative pitch angle and conversion efficiency in the period region of $T(g/h)^{0.5} < 4.4$, on the contrary, efficiency is sensitive to WEC draft variations in the long-period waves ($4.4 < T(g/h)^{0.5}$) which has strong transmission. This is because the increased WEC draft hinders the transmission of long waves and raises the components of wave extraction and reflection, as shown in Fig. 10(e) and Fig. 10(f). It should be noticed that as the draft of the WEC decreases, the resonant period of the second peak in the conversion efficiency becomes smaller. This phenomenon is constructive which proves that the proposed integrated system can obtain more stable efficiency in irregular waves of practical engineering by increasing WEC draft.

4.5. Effect of the WEC bottom shape

Different bottom shapes can change the vorticity field around the WEC, which affects the hydrodynamic performance of the integrated system in turn. This sub-section studies the influence of WEC bottom shape on wave energy extraction performance and wave attenuation performance of the hybrid system. As shown in Fig. 11, four different WEC bottom shapes are considered, they are square bottom, semi-circular bottom and two mirrored asymmetric cambered bottoms A and B. The difference between asymmetric cambered bottoms A and B is that the concave surfaces are located on the back wave side and the wave side of the WEC, respectively.

Their width and draft were kept the same. The other parameters remain unchanged from Section 4.1. Fig. 12 shows the variation of the relative pitch RAO ξ/h, conversion efficiency η, rotated RAO of WEC ξ_w/h, rotated RAO of breakwater ξ_b/h, reflection coefficient K_r and transmission coefficient K_t with wave periods for different WEC bottoms. The vorticity fields around the four WECs with different bottom shapes are shown in Fig. 12.

The first peaks in the efficiency of the hybrid systems with four different WEC bottom shapes occur at the same period, but the second peaks have different values at different periods. It can be concluded that the change in the shape of the WEC bottom affects the magnitude of the second efficiency peak of the system and the wave period in which it is located, due to the fact that the weight and the resonant period of the WEC are changed with the variation in the shape of the bottom. From the perspective of wave energy conversion, among the four different models in this sub-section, the same symmetrical shape of the square bottom and the semi-circular bottom perform better in all of the test wave periods. This is attributed to that wave energy is collected by the back-forth oscillating of the WEC, and the symmetrical bottom shape allows the WEC to be subjected to less resistance in motion. The conversion efficiencies of the two systems with asymmetric WEC bottom shapes are similar. Within the period range of $6.7 < T(g/h)^{0.5}$, the conversion efficiency of asymmetric bottom A exceeds that of asymmetric bottom B. This phenomenon may be attributed to the smooth convex surface on the wave-facing side of asymmetric bottom A, facilitating a more effective capture of wave energy by the WEC. This leads to greater rotational motion of the WEC and larger relative pitch angles, as illustrated in Fig. 12(a) and (c). Next, the two bottoms of symmetrical shapes are first analyzed in comparison.

It can be seen that the conversion efficiencies of the two symmetrically bottom-shaped hybrid systems almost overlap at the first peak with a value of 32 %. However, the second peak efficiency of the system with a semi-circular bottom WEC is 30 % higher than that of the other WEC and moves towards the short-wave region. It is noteworthy that the valley of conversion efficiency between the two peaks remains and also

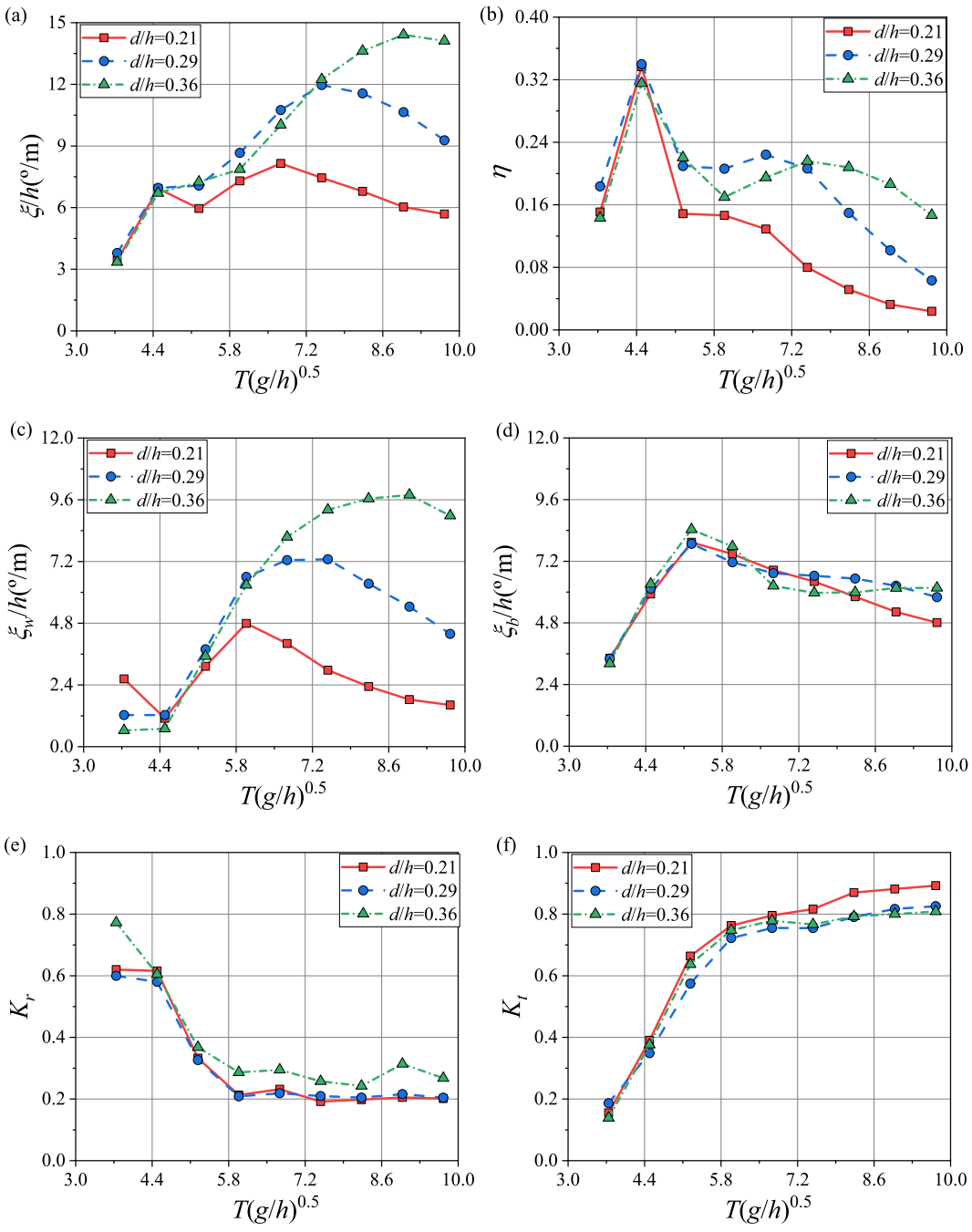

Fig. 10. Variation of (a) relative pitch angle, (b) conversion efficiency, (c) rotated angle of WEC, (d) rotated angle of breakwater, (e) reflection coefficient and (f) transmission coefficient with wave periods at varying WEC drafts.

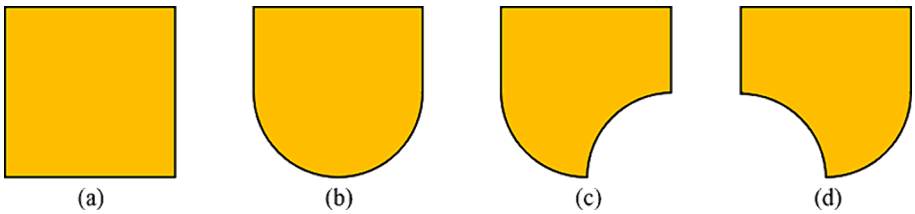

Fig. 11. Schematic diagram of four WECs with different bottom shapes (a) square bottom, (b) semi-circular bottom, (c) asymmetric cambered bottom A and (d) asymmetric cambered bottom B.

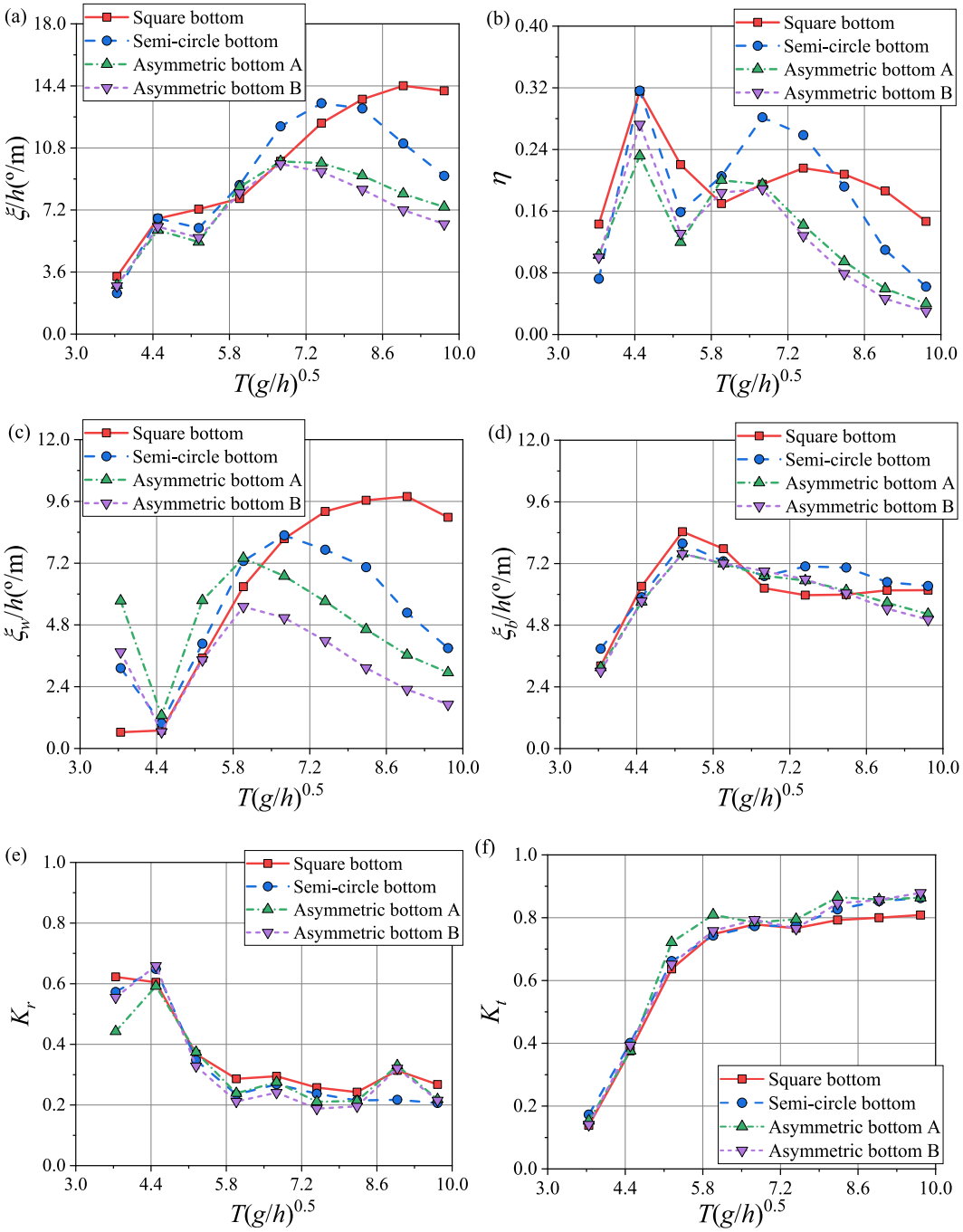

Fig. 12. Comparisons are made between the four types of hybrid systems with differing bottom shapes in terms of (a) relative pitch angle, (b) conversion efficiency, (c) rotated angle of WEC, (d) rotated angle of breakwater, (e) reflection coefficient, and (f) transmission coefficient.

shifts to the short-wave region. It can be summarized that replacing the square-bottom WEC with the semi-circle bottom WEC results in a narrow effective frequency bandwidth of the second peak, but the peak efficiency and the wave frequency at which the peak efficiency is located will be promoted.

As plotted in Fig. 12(c), the rotated angle of the semicircular WEC is larger than that of the square-bottom WEC in short-period waves ($T(g/h)^{0.5} > 6.7$) and shows the opposite trend in long-period waves. This is since that the semicircular bottom shape favours wave energy extraction in short-period waves, whereas in long waves the semicircular bottom shape is more conducive to fluid transmission over the WEC. Therefore, Fig. 12(d) presents inverse characteristics as those in Fig. 12(c). That is, for a semicircular bottom, long waves are more likely to be transmitted over the WEC and increase the motion of the breakwater. Finally, the square bottom corresponds to a greater reflection coefficient and a smaller transmission coefficient, as the straight walls of the square WEC have a better damping effect on the waves.

Fig. 13(a)-(d) shows that there are stronger vortices near the corner of the square bottom than the semi-circle bottom so less energy is dissipated for the WEC with the semi-circle bottom. The semi-circular bottom is smooth and beneficial to wave transmission, consequently, most of the energy is transferred to the breakwater, leading to more intense vortices at breakwater corners. When the two asymmetric WECs move, only small vortices are shed near the recesses and the corners. In addition to this, the asymmetric bottom A has higher efficiency than B due to the concave surface which on the wave-facing side can lead to

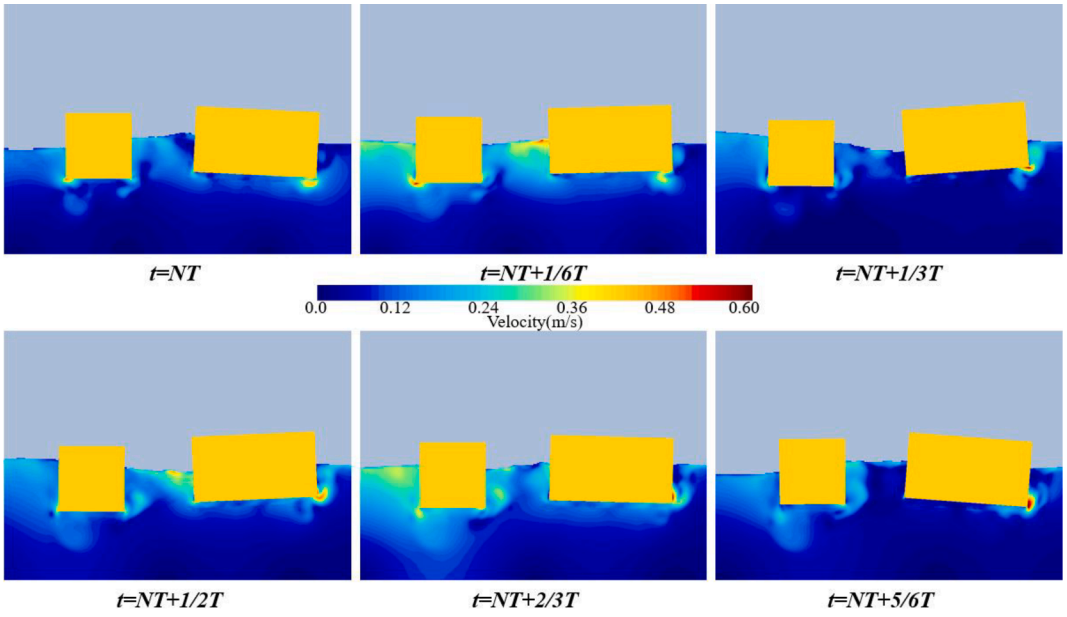

(a) Square bottom

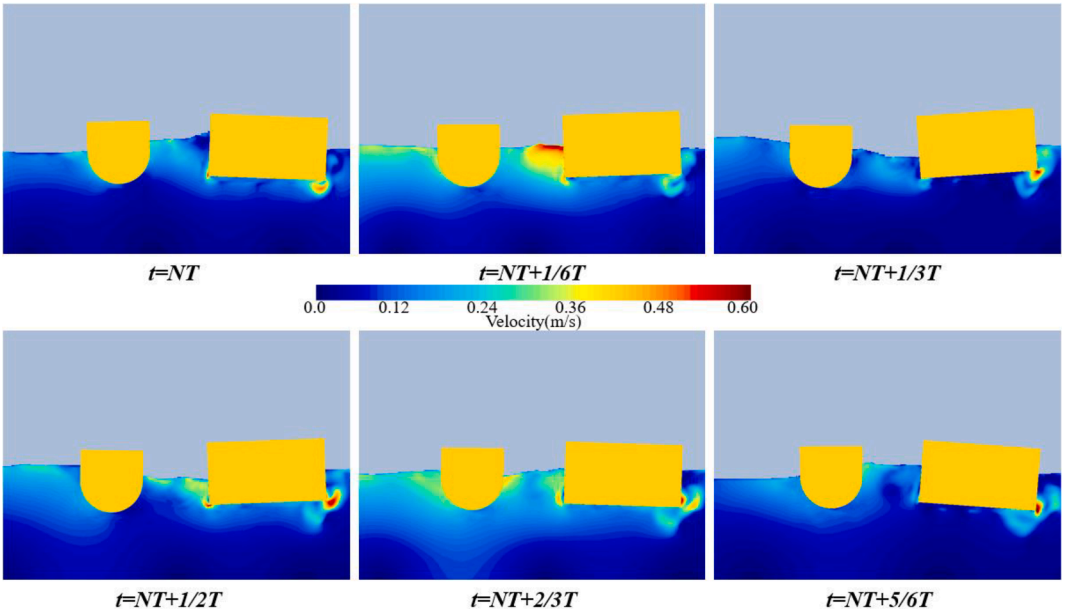

(b) Semi-circle bottom

Fig. 13. Vorticity fields around the two WECs with different bottom shapes.

more pronounced vortex dissipation.

From the above comparison, it can be seen that the hybrid system with square bottom WEC has favorable effective frequency bandwidth and wave extraction performance. However, the peak efficiency of the semi-circle bottom is more prominent. Both of these WECs with simpler bottom construction have better energy extraction performance, meaning that the Levelised Cost of Electricity (LCoE) will be lower in practical engineering applications. The findings in this sub-section provide valuable recommendations for optimizing the geometric WEC shape of WEC-breakwater systems for real applications.

5. Conclusions

Broadening the effective frequency bandwidth and improving wave attenuation in long-period waves are two important aspects that drive the commercialization of WECs and floating breakwaters. To optimize the design parameters of the WEC-breakwater hybrid system, the effects of caisson width, sub-devices distance, WEC draft and WEC bottom shape on the coupled hydrodynamic performance of the system are explored. The hybrid system consists of a floating breakwater and a WEC, generating electricity by the relative motion of the two devices under wave loads. An accurate CFD model was proposed to study the interaction of the integrated system with waves and the superiority of

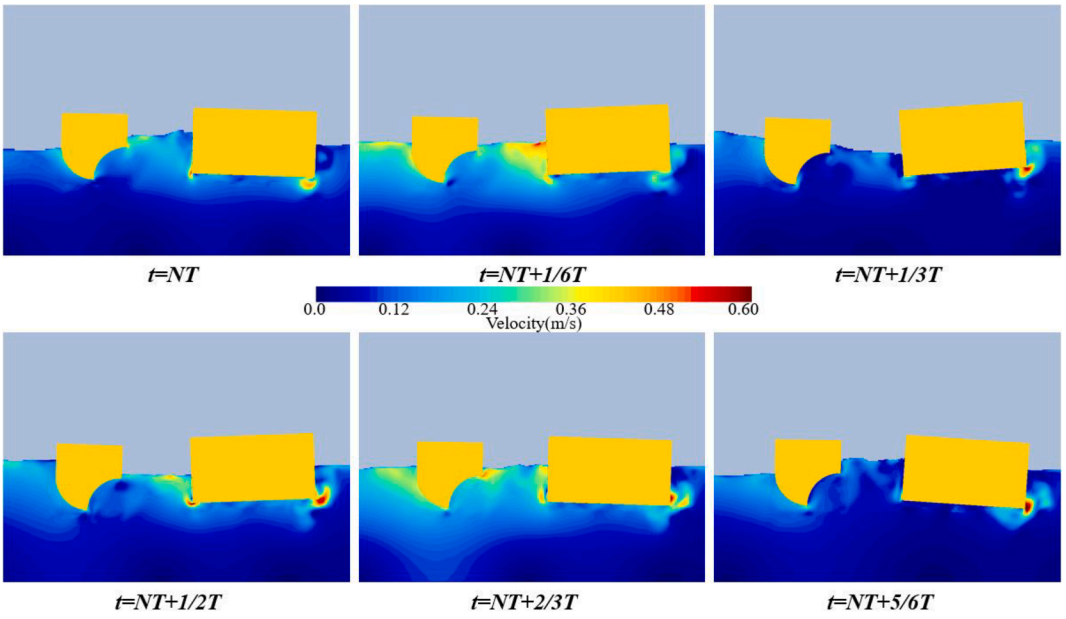

(c) Asymmetric cambered bottom A

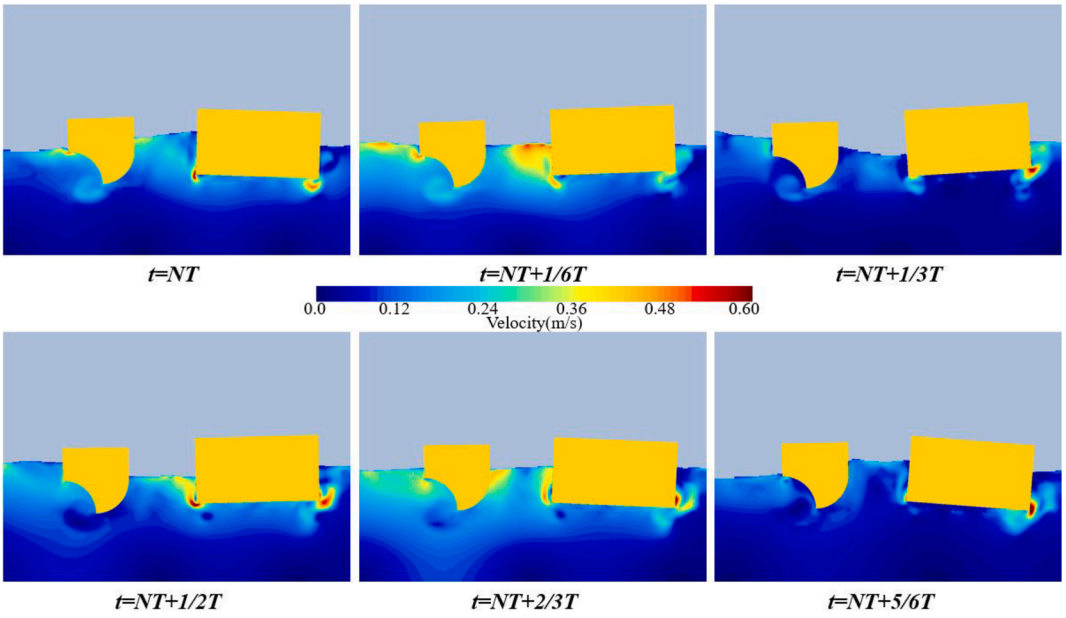

(d) Asymmetric cambered bottom B

Fig. 13. (*continued*).

the optimized floating hybrid system is validated in terms of energy capture and wave protection. Some main findings are summarized as follows

(1) Adding side rectangular caissons to the breakwater has a positive effect on the performance in long-period waves. This is because the wave clustering effect of the formed chamber structure which increases the energy density inside it. Moreover, the resonance of chamber water causes more energy dissipation, which in turn reduces the wave loads and improves the reliability.
(2) The maximum conversion efficiency of the combination remains around 35 %, regardless of changes in side caisson width. However, near the resonant period of the water column inside the chamber, increasing the side caisson width decreases the volume of the water column, inducing lower energy losses. Considering energy conversion efficiency and wave absorption, the hybrid system with a larger caisson width is a better choice.
(3) The layout position of the WEC can have a significant effect on its motion, but this change is not necessarily reflected in the conversion efficiency. This is because the conversion efficiency is relevant to the relative pitch angle of the two sub-devices, which is jointly determined by both devices.
(4) Changing the WEC draft has a small influence on the motion response of the system in short-period waves, but deeper drafts have a strong retardation effect on long waves. To some extent,

the larger draft WEC allows for more effective energy capture for long-period waves.

(5) The effective wave period region and maximum efficiency of the system near the second efficiency peak can be increased by adjusting the WEC bottom shape. For four different bottom shapes of WECs, the symmetric bottom has more outstanding energy conversion performance than the asymmetric bottom in long waves because of the weaker resistance. In particular, the efficiency of the semi-circle bottom WEC can reach 28 %, which is more than 30 % higher than asymmetric bottoms. As far as the wave dissipation performance, the more intense vortices at the corners of the square WEC result in a smaller transmission coefficient for the system.

The coupling motion including the heaving and pitching of the developed WEC-breakwater numerical model, and the energy capture performance wave absorption characteristics of the hybrid system are studied. Afterward, parameters including side caisson width, sub-devices spacing, WEC draft and WEC bottom shape are further discussed. The results of this study are important to simulate the motion patterns of WEC-breakwater systems more accurately in practical engineering, which can enhance the optimized design of WEC systems.

CRediT authorship contribution statement

Fukai Song: Writing – original draft, Validation, Investigation, Formal analysis. **Yong Cheng:** Writing – original draft, Supervision, Software, Methodology, Data curation. **Saishuai Dai:** Writing – review & editing, Supervision, Formal analysis, Data curation. **Zhiming Yuan:** Writing – review & editing. **Atilla Incecik:** Supervision, Funding acquisition.

Declaration of competing interest

The authors declare that they have no known competing financial interests or personal relationships that could have appeared to influence the work reported in this paper.

Data availability

Data will be made available on request.

Acknowledgment

The authors are grateful to the National Natural Science Foundation of China (Grant No. 52271278, 52111530137), Natural Science Found of Jiangsu Province (Grant No. BK20221389), Postgraduate Research & Practice Innovation Programme of Jiangsu Province (Grant No. SJCX23_2213) and the Newton Advanced Fellowships (Grant No. NAF \R1\180304) by the Royal Society for supporting this work.

References

[1] World Wide Fund For Nature (WWF), 2023. See https://www.wwfchina.org/work?id=3.
[2] COM(2020)741-EU Strategy to Harness the Potential of Offshore Renewable Energy for a Climate Neutral Future-EU Monitor. See https://www.eumonitor.eu/9353000/1/j9vvik7m1c3gyxp/vldwjbykscwq.
[3] Oliveira-Pinto S, Rosa-Santos P, Taveira-Pinto F. Assessment of the potential of combining wave and solar energy resources to power supply worldwide offshore oil and gas platforms. Energy Convers Manage 2020;223:113299.
[4] Ocean Energy Systems (OES). OES annual reports 2010-2019. See https://www.ocean-energy-systems.org/publications/oes-annual-reports/document/oes-annual-report-2010-2019/.
[5] Wave Swell Energy. Uniwave. See https://www.waveswell.com/technology/.
[6] Ning DZ, Zhou Y, Mayon D, Johanning L. Experimental investigation on the hydrodynamic performance of a cylindrical dual-chamber Oscillating Water Column device. Appl Energy 2019;260:114252.
[7] AW-Energy. WaveRoller. See https://aw-energy.com/waveroller/.
[8] Zheng XB, Ji MZ, Jing FM, Lu Y, Zheng WH, Zhou SH, et al. Sea trial test on offshore integration of an oscillating buoy wave energy device and floating breakwater. Energy Convers Manage 2022;256:153775.
[9] Ocean Energy Europe (OEE). Final LAMWEC tank tests complete prior to EMEC deploym ent. See https://www.oceanenergy-europe.eu/industry-news/final-lamwec-tank-tests-complete-prior-to-emec-deployment/.
[10] Ozkop E, Altas IH. Control, power and electrical components in wave energy conversion systems: a review of the technologies. Renew Sustain Energy Rev 2017;67:106–15.
[11] Zhang HM, Zhou B, Vogel C, Willden R, Zang J, Zhang L. Hydrodynamic performance of a floating breakwater as an oscillating-buoy type wave energy converter. Appl Energy 2020;257:113996.
[12] Ning DZ, Zhao XL, Göteman M, Kang HG. Hydrodynamic performance of a pile-restrained WEC-type floating breakwater: An experimental study. Renew Energy 2016;95:531–41.
[13] Sun L, Zang J, Stansby P, Carpintero E, Moreno E, Taylor PH, et al. Linear diffraction analysis of the three-float multi-mode wave energy converter M4 for power capture and structural analysis in irregular waves with experimental validation. J Ocean Eng Mar Energy 2017;3:51–68.
[14] Carpintero ME, Stansby P. The 6-float wave energy converter M4: Ocean basin tests giving capture width, response and energy yield for several sites. Renew Sustain Energy Rev 2019;104:307–18.
[15] Santo H, Taylor PH, Stansby PK. The performance of the three-float M4 wave energy converter off Albany, on the south coast of western Australia, compared to Orkney (EMEC) in the U.K. Renew. Energy 2019;146:444–59.
[16] Zheng SM, Zhang YL, Sheng WA. Maximum Wave energy conversion by two interconnected floaters. J Energy Resour Technol 2016;138:032004.
[17] Zheng SM, Zhang YL. Analysis for wave power capture capacity of two interconnected floats in regular waves. J Fluid Struct 2017;75:158–73.
[18] Yu D, Wang KY, Liu HX, Kong FK, Yang C, Duan YP, et al. Investigation on motion characteristics of an Anti-pitching Generating WEC (AGWEC) considering the viscous effect. Ocean Eng 2022;246:110619.
[19] Wang LG, Wu SX, Huang TH, Chen WC. On improving the wave-to-wire efficiency of a two-body hinge-barge wave energy converter. Ocean Eng 2023;278:114388.
[20] Wave Star AS. Wave Star energy web page. In: Wave star AS. 2012.
[21] Ren NX, Ma Z, Fan TH, Zhai GJ, Ou JP. Experimental and numerical study of hydrodynamic responses of a new combined monopile wind turbine and a heave-type wave energy converter under typical operational conditions. Ocean Eng 2018;159:1–8.
[22] Ren NX, Ma Z, Shan BH, Ning DZ, Ou JP. Experimental and numerical study of dynamic responses of a new combined TLP type floating wind turbine and a wave energy converter under operational conditions. Renew Energy 2020;151:966–74.
[23] Wan L, Ren NX, Zhang PY. Numerical investigation on the dynamic responses of three integrated concepts of offshore wind and wave energy converter. Ocean Eng 2020;217:107896.
[24] Zhou BZ, Hu JJ, Jin P, Sun K, Li Y, Ning DZ. Power performance and motion response of a floating wind platform and multiple heaving wave energy converters hybrid system. Energy 2023;265:126314.
[25] Cheng Y, Dai SQ, Dai SS, Ji CY, Collu M, Yuan ZM, et al. Energy conversion and hydrodynamic analysis of multi-degree-of-freedom wave energy converters integrated into a semi-submersible platform. Energy Convers Manage 2022;252:115075.
[26] Tian WJ, Wang YP, Shi W, Michailides C, Wan L, Chen MS. Numerical study of hydrodynamic responses for a combined concept of semisubmersible wind turbine and different layouts of a wave energy converter. Ocean Eng 2023;272:113824.
[27] He F, Huang ZH, Law WK. An experimental study of a floating breakwater with asymmetric pneumatic chambers for wave energy extraction. Appl Energy 2013;106:222–31.
[28] Zhang HM, Zhou BZ, Vogel C, Wilden R, Zang J, Geng J. Hydrodynamic performance of a dual-floater hybrid system combining a floating breakwater and an oscillating-buoy type wave energy converter. Appl Energy 2020;259:114212.
[29] Yang I, Tezdogan T, Incecik A. Numerical investigations of a pivoted point absorber wave energy converter integrated with breakwater using CFD. Ocean Eng 2023;274:114025.
[30] Cheng Y, Fu L, Dai SS, Collu M, Ji CY, Yuan ZM, et al. Experimental and numerical investigation of WEC-type floating breakwaters: A single-pontoon oscillating buoy and a dual-pontoon oscillating water column. Coastal Eng 2022;177:104188.
[31] Ji QL, Xu CH, Jiao CS. Numerical investigation on the hydrodynamic performance of a vertical pile-restrained reversed L type floating breakwater integrated with WEC. Ocean Eng 2021;238:109635.
[32] Cheng Y, Xi C, Dai SS, Ji CY, Cocard M, Yuan ZM, et al. Performance characteristics and parametric analysis of a novel multi-purpose platform combining a moonpool-type floating breakwater and an array of wave energy converters. Appl Energy 2021;292:116888.
[33] Cheng Y, Fu L, Dai SS, Collu M, Cui L, Yuan ZM, et al. Experimental and numerical analysis of a hybrid WEC-breakwater system combining an oscillating water column and an oscillating buoy. Renew Sustain Energy Rev 2022;169:112909.
[34] Madhi F, Sinclair ME, Yeung RW. The "Berkeley wedge": an asymmetrical energy-capturing floating breakwater of high performance. Marine Syst Ocean Tech 2014;9(1):5–16.
[35] Tay ZY. Performance and wave impact of an integrated multi-raft wave energy converter with floating breakwater for tropical climate. Ocean Eng 2020;218:108136.
[36] Zhang HM, Zhou BZ, Zang J, Vogel C, Jin P, Ning DZ. Optimization of a three-dimensional hybrid system combining a floating breakwater and a wave energy converter array. Energy Convers Manage 2021;247:114717.

[37] Tay ZY. Effect of resonance and wave reflection in semi-enclosed moonpool on performance enhancement of point absorber arrays. Ocean Eng 2022;243:110182.
[38] Tay ZY. Energy generation enhancement of arrays of point absorber wave energy converters via Moonpool's resonance effect. Renew Energy 2022;188:830–48.
[39] Fenton JD. A fifth-order stokes theory for steady waves. J Waterw Port, Coast Ocean Eng 1985;111(2):216–34.
[40] Kim J, O'Sullivan J, Read A. Ringing analysis of a vertical cylinder by euler overlay method. In: ASME 2012 31st International Conference on Ocean, Offshore and Arctic Engineering. American Society of Mechanical Engineers; 2012. p. 855–66.
[41] Choi J, Yoon SB. Numerical simulations using momentum source wave-maker applied to RANS equation model. Coastal Eng 2009;56:1043–60.
[42] Simonsen CD, Otzen JF, Joncquez S, Stern F. EFD and CFD for KCS heaving and pitching in regular head waves. J Mar Sci Tech-Japan 2013;18(4):435–59.
[43] Jin SY, Wang DM, Hann M, Collins K, Conley D, Greaves D. A designed two-body hinged raft wave energy converter: From experimental study to annual power prediction for the EMEC site using WEC-Sim. Ocean Eng 2023;267:113286.
[44] Wang XY, Liu Y, Lu L. Analytical solution of oblique wave interacting with a periodic array of specific caissons connected with partially immersed thin walls (comb-type). Ocean Eng 2019;186:106107.
[45] Zhao XL, Zhang Y, Li MW, Johanning L. Hydrodynamic performance of a Comb-Type Breakwater-WEC system: An analytical study. Renew Energy 2020;159:33–49.
[46] Zhao XL, Zhang Y, Li MW, Johanning L. Experimental and analytical investigation on hydrodynamic performance of the comb-type breakwater-wave energy converter system with a flange. Renew Energy 2021;172:392–407.